High responsivity sensing of unfocused laser and white light using graphene photodetectors grown by chemical vapor deposition

Downloaded from: https://research.chalmers.se, 2025-12-10 00:27 UTC

Citation for the original published paper (version of record):
Liu, Q., Deng, J., Xu, C. et al (2016). High responsivity sensing of unfocused laser and white light using graphene photodetectors
grown by chemical vapor deposition. Optical Materials Express, 6(7): 2158-2164.
http://dx.doi.org/10.1364/OME.6.002158

N.B. When citing this work, cite the original published paper.

research.chalmers.se offers the possibility of retrieving research publications produced at Chalmers University of Technology. It covers all kind of research output: articles, dissertations, conference papers, reports etc. since 2004. research.chalmers.se is administrated and maintained by Chalmers Library

(article starts on next page)

High responsivity sensing of unfocused laser and white light using graphene photodetectors grown by chemical vapor deposition

Qi Liu,[1] Jun Deng,[1] Chen Xu,[1,3] Yiyang Xie,[1] Yibo Dong,[1] Guanzhong Pan,[1] and Jie Sun[1,2,4]

[1]*Key Laboratory of Optoelectronics Technology, School of Electronic Information and Control Engineering, Beijing University of Technology, Beijing 100124, China*

[2]*Department of Microtechnology and Nanoscience, Chalmers University of Technology, Gothenburg 41296, Sweden*

[3]*xuchen58@bjut.edu.cn*

[4]*jie.sun@chalmers.se*

Abstract: Graphene photodetectors grown by chemical vapor deposition are fabricated for unfocused laser and white light sensing. The unfocused light enlarges the illuminated graphene area and mimics the real-life sensing conditions, yielding a responsivity of 104 mA/W at room temperature without enhancing absorbance by waveguide and plasmonics. The devices are based on positive photoconductivity from the electron-hole photocarrier pairs and the bolometric-effect-induced negative photoconductivity. The buried off-center local gate induces a net internal potential in the graphene. The relative strength of the two photoconductivities depends on the gate voltage. The technology is scalable, which is a step ahead toward real applications.

©2016 Optical Society of America

OCIS codes: (160.4236) Nanomaterials; (230.5160) Photodetectors.

References and links

1. Q. Bao and K. P. Loh, "Graphene photonics, plasmonics, and broadband optoelectronic devices," ACS Nano **6**(5), 3677–3694 (2012).
2. M. Thomas, F. Xia, and P. Avouris, "Graphene photodetectors for high-speed optical communications," Nat. Photonics **4**(5), 297–301 (2010).
3. A. Pospischil, M. Humer, M. M. Furchi, D. Bachmann, R. Guider, T. Fromherz, and T. Mueller, "CMOS-compatible graphene photodetector covering all optical communication bands," Nat. Photonics **7**(11), 892–896 (2013).
4. X. Gan, R.-J. Shiue, Y. Gao, I. Meric, T. F. Heinz, K. Shepard, J. Hone, S. Assefa, and D. Englund, "Chip-integrated ultrafast graphene photodetector with high responsivity," Nat. Photonics **7**(11), 883–887 (2013).
5. C. Chakraborty, R. Beams, K. M. Goodfellow, G. W. Wicks, L. Novotny, and A. N. Vamivakas, "Optical antenna enhanced graphene photodetector," Appl. Phys. Lett. **105**(24), 241114 (2014).
6. M. Freitag, T. Low, F. Xia, and P. Avouris, "Photoconductivity of biased graphene," Nat. Photonics **7**(1), 53–59 (2012).
7. X. Cai, A. B. Sushkov, R. J. Suess, M. M. Jadidi, G. S. Jenkins, L. O. Nyakiti, R. L. Myers-Ward, S. Li, J. Yan, D. K. Gaskill, T. E. Murphy, H. D. Drew, and M. S. Fuhrer, "Sensitive room-temperature terahertz detection via the photothermoelectric effect in graphene," Nat. Nanotechnol. **9**(10), 814–819 (2014).
8. N. M. Gabor, J. C. W. Song, Q. Ma, N. L. Nair, T. Taychatanapat, K. Watanabe, T. Taniguchi, L. S. Levitov, and P. Jarillo-Herrero, "Hot carrier-assisted intrinsic photoresponse in graphene," Science **334**(6056), 648–652 (2011).
9. X. Kun, X. Chen, D. Jun, Z. Yanxu, G. Weiling, M. Mingming, Z. Lei, and S. Jie, "Graphene transparent electrodes grown by rapid chemical vapor deposition with ultrathin indium tin oxide contact layers for GaN light emitting diodes," Appl. Phys. Lett. **102**(16), 162102 (2013).
10. K. Xu, C. Xu, Y. Xie, J. Deng, Y. Zhu, W. Guo, M. Xun, K. B. K. Teo, H. Chen, and J. Sun, "Graphene GaN-based Schottky ultraviolet detectors," IEEE Trans. Electron Dev. **62**(9), 2802–2808 (2015).
11. J. Sun, N. Lindvall, M. T. Cole, K. T. T. Angel, T. Wang, K. B. K. Teo, D. H. C. Chua, J. Liu, and A. Yurgens, "Low partial pressure chemical vapor deposition of graphene on copper," IEEE Trans. NanoTechnol. **11**(2), 255–260 (2012).

#262435 Received 4 Apr 2016; revised 24 May 2016; accepted 24 May 2016; published 1 Jun 2016

12. C. J. L. de la Rosa, J. Sun, N. Lindvall, M. T. Cole, Y. Nam, M. Löffler, E. Olsson, K. B. K. Teo, and A. Yurgens, "Frame assisted H_2O electrolysis induced H_2 bubbling transfer of large area graphene grown by chemical vapor deposition on Cu," Appl. Phys. Lett. **102**(2), 022101 (2013).
13. L. Liu, X. Liu, Z. Zhan, W. Guo, C. Xu, J. Deng, D. Chakarov, P. Hyldgaard, E. Schröder, A. Yurgens, and J. Sun, "A mechanism for highly efficient electrochemical bubbling delamination of CVD-grown graphene from metal substrates," Adv. Mater. Interfaces **3**, 1500492 (2016).
14. R. Shi, H. Xu, B. Chen, Z. Zhang, and L.-M. Peng, "Scalable fabrication of graphene devices through photolithography," Appl. Phys. Lett. **102**(11), 113102 (2013).
15. F. Xia, T. Mueller, R. Golizadeh-Mojarad, M. Freitag, Y. M. Lin, J. Tsang, V. Perebeinos, and P. Avouris, "Photocurrent imaging and efficient photon detection in a graphene transistor," Nano Lett. **9**(3), 1039–1044 (2009).

1. Introduction

Graphene, a conjugated sp^2 carbon two-dimensional (2D) crystal, possesses many outstanding properties and has received a lot of interest. In particular, the potential applications in nanoscale electronics and photonics are appealing. It has super high electrical and thermal conductivity, carrier mobility, optical transmittance with a wide spectral range, chemical stability and mechanical strength. While there exist competitors regarding each of the properties, it is almost impossible to find an alternative material that integrates all these aspects within a single atomic sheet. Graphene integrated with silicon may be the key enabling technology in the next generation complementary metal-oxide-semiconductor compatible photonics and optoelectronics [1].For example, on Si, graphene photodetectors with high-speed and wide spectral operation are demonstrated [2,3], thanks to its high mobility and gapless energy band. It is fundamentally advantageous over traditional semiconductor based photodetectors, where the mobility is usually orders of magnitude lower, and the absorption spectra have a "long wavelength limit" due to the bandgap. The drawbacks of graphene detectors are mainly the weak absorption of the incident light as a result of the atomic thickness. This issue, however, is not the limiting factor. The coupling between the graphene and light can be compensated, to a large extent, by auxiliary techniques such as integrating a waveguide [4], enhancing the field by plasmonic effect [5], etc.

To date, the mechanism of graphene photodetectors is not well understood. Photodetectors can be categorized into two classes by whether an electromotive force $\mathcal{E}$ is produced or not. The devices that generate electromotive forces can be roughly divided into two types: classical photovoltaic devices and thermoelectric devices. The photovoltaic devices rely on the photon induced electron-hole (e-h) pairs which are collected by the electrodes [6]. The thermoelectric Seebeck effect is induced by the light created temperature gradient in the device, together with the inhomogeneity in the graphene [7]. Both mechanisms can be enhanced by hot carriers, which lose energy to the lattice slowly, but rapidly relax energy by electron-electron (e-e) scattering [8]. A photocurrent may be seen even without a bias. The other category of photodetectors refers to those without $\mathcal{E}$. In other words, to observe a photocurrent, an external bias voltage is a must. Largely, the devices can also be divided into two groups: those based on traditional photoconductivity (TP) and those on bolometric effect. The incident light generates e-h pairs in the graphene, leading to the enhanced conductivity (TP). The bolometric effect is due to the temperature-dependent resistance of graphene. When heat is generated in the sample, due to the pronounced e-e scattering, the carrier mobility goes down, resulting in a negative photoconductivity.

Currently in literature, graphene photodetector is dominantly fabricated in micro exfoliated graphene, and the light source is mainly focused laser beam (typical spot size 3-6 μm with a power density of several 100 kW/cm^2, yielding a responsivity of few mA/W) [2]. In this letter, graphene transistors with buried local gate are fabricated and used as photodetectors. Distinct from most other research, the devices are prepared in chemical vapor deposited (CVD) graphene which can be processed reproducibly in arrays. The technique is scalable, holding high potential for industrialization. Also, as mentioned before, a drawback for graphene light sensors is their low absorbance. Thus, here unfocused laser and white light

#262435 Received 4 Apr 2016; revised 24 May 2016; accepted 24 May 2016; published 1 Jun 2016
© 2016 OSA

is used instead of focused beam. It is more similar to the real-life light sensing environment, and more importantly, at a given optical power, the photosensitive surface is greatly enlarged. The photocurrent, hence the responsivity R = I/W, is increased. Therefore, although there is no absorption improving elements e.g. waveguide in the devices, a very large R can be achieved (104 mA/W). The devices work at small source-drain voltages, and the performance is explained by the competing mechanisms of TP and bolometric effects. The work contributes to the understanding of the physics of graphene photo response, and is a step forward to real applications.

2. Experiment

The graphene is grown by cold wall Aixtron high temperature CVD on Cu foils with a similar recipe to our previous work [9–13]. The device layout is shown in Fig. 1, where (a) is the lithographic pattern and (b) is the schematic illustration. The detector is fabricated by three-step lithography on a Si substrate with 300 nm SiO_2 layer. First, inductively coupled plasma is used to etch a 90 μm × 450 μm × 90 nm trench in the SiO_2. 90 nm Ti/Au (the same as the trench depth) is sputtered into the trench to form the gate. Another 300 nm SiO_2 film is grown by plasma enhanced CVD as the gate dielectric. Second, the 15/30 nm Ti/Au source and drain contacts are prepared by lift-off. Finally, the monolayer graphene is transferred to the chip by etching away the Cu with a solution of $CuSO_4$:HCl (concentrated):H_2O = 15 g:50 ml: 50 ml, and patterned to 50 μm × 350 μm.

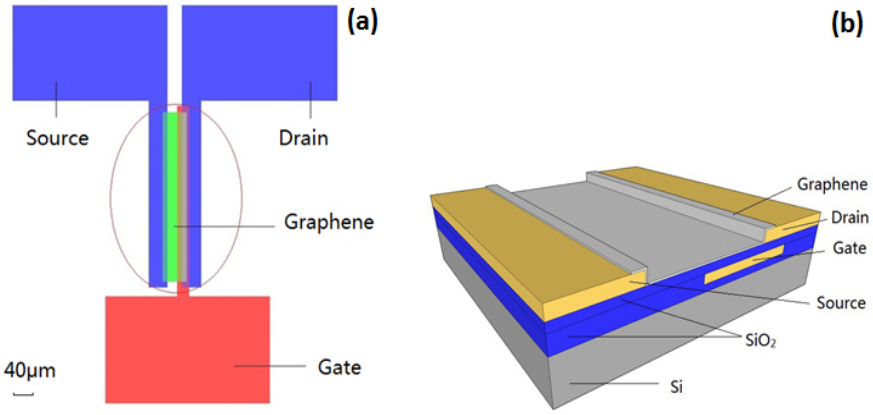

Fig. 1. (a) Mask patterns (drawn to scale) used in the device fabrication (three-step photolithography). (b) Schematic illustration of the graphene transistor. The buried gate is placed off-center and has a small overlap with the drain to introduce a net potential in the channel.

A typical Raman spectrum is shown in Fig. 2(a). The D peak is small, indicating the quality of the graphene is reasonably high. The narrow 2D peak is ~2 times as high as the G peak, implying that the as-deposited graphene is a monolayer. Figure 2(b) shows the room temperature transfer characteristics of the fabricated graphene transistor. The Dirac point is at V_g = 20 V (Unless otherwise specified, in this letter whenever we talk about graphene we refer to the part that is controlled by the local gate). Using a capacitor based simple model, the carrier mobility is estimated to be ~750 $cm^2/(Vs)$. The *p*-doping and moderate mobility are ascribed to the photolithography process, which is known to dope graphene and introduce scatterers [14]. The light sources used in the experiments are 790 nm laser (500 mW/cm^2) and white light emitting diodes (LED, 12 W), which are placed ~10 cm above the graphene and the whole graphene is within the illuminated area. All the measurements are carried out at ambient condition with no special treatment (e.g. annealing, vacuum, low temperature), and the source is grounded.

#262435 Received 4 Apr 2016; revised 24 May 2016; accepted 24 May 2016; published 1 Jun 2016
© 2016 OSA

Figure 2(c) shows the dark *I-V* curves at several different V_g. Because the Dirac point is at V_g = 20 V, the linear *I-V* curve at this gate voltage shows the lowest conductance, in agreement with Fig. 2(b). At decreased or increased V_g, the graphene is *p*- or *n*-type doped, and the conductance increases. Figure 2(d) demonstrates the light sensing experiment performed at two typical gate voltages (V_g = 20 V and V_g = 0 V).

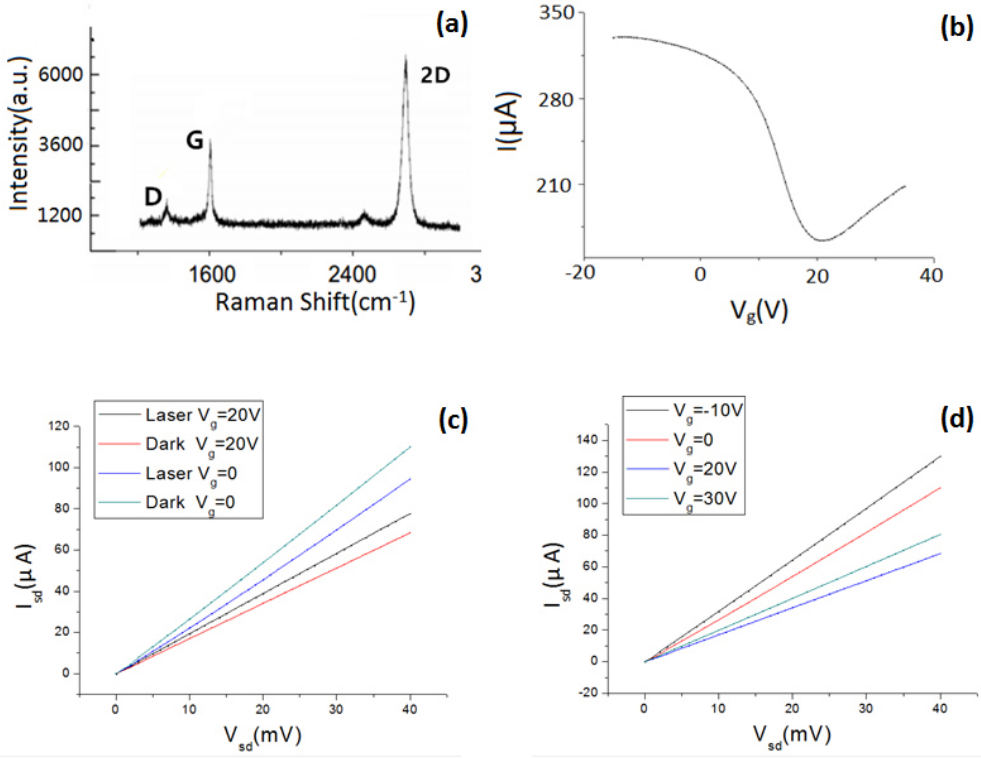

Fig. 2. (a) Typical Raman spectrum of the graphene transferred to SiO_2/Si. (b) Typical room temperature gate curve of the graphene transistor fabricated by three-step photolithography. (c) I-V curves of the transistor at several different gate voltages. When V_g = 20 V ("Dirac voltage") the device shows the lowest current. (d) I-V curves of the device with and without laser illumination when V_g = 20 V and 0 V.

When the laser is on, there are clear photo responses. Nevertheless, the photocurrents are of opposite signs in the two cases. In order to further dig into the problem, photo detection at fixed V_{sd} is done while sweeping V_g, as plotted in Fig. 3, where (a) and (b) show the photocurrent illuminated by laser and white light ($I_{ph\text{-}laser}$ and $I_{ph\text{-}white}$), respectively. Despite the different scale of the ordinates, the curves in Fig. 3(a) and 3(b) have similar shapes. The photocurrents, defined as $I_{ph} = I_{light}\text{-}I_{dark}$, are positive when V_g is around 20 V, turn negative when V_g is decreased to around 0 V, and finally return to almost zero when V_g is deeply negative. The responsivity is considerably large. *R* reaches its peak value of 0.104 A/W for 790 nm laser illumination at V_{sd} of merely 0.04 V (V_g = 20 V). The complicated behavior in Fig. 3 seems hard to understand at a first glance. However, below we show it can be well explained by the competition between the TP and bolometric effects at various V_g.

#262435 Received 4 Apr 2016; revised 24 May 2016; accepted 24 May 2016; published 1 Jun 2016
© 2016 OSA

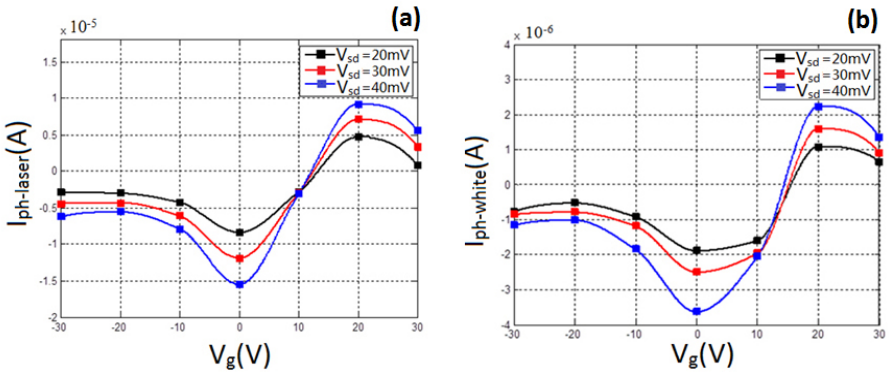

Fig. 3. Photo response of the device at room temperature when illuminated by unfocused (a) 790 nm laser and (b) white LED. The two figures are qualitatively similar. There are three regimes of the operation. Region 1: V_g is around 20 V and the device shows positive photoconductivity (TP dominating); region 2: V_g is around 0 V showing negative photoconductivity (bolometric photoconductivity dominating); and region 3: V_g is less than ~10 V with much more reduced photo response (TP and bolometric effects balancing out).

3. Discussion

First we compute the potential profile of the graphene. In our device, the graphene and the gate form a capacitor, which can be viewed as the geometry capacitance C_O and the quantum capacitance C_Q connected in series. If V_D is the Dirac voltage (gate voltage at which the graphene is intrinsic, in our case V_D = 20 V), we can define $V_g' = |V_g - V_D|$ (For convenience, in Eqs. (1), (2) and (3) all letters are absolute values). We have

$$V_g' = V_O + V_Q, \tag{1}$$

where the latter two items are the voltages across the two capacitors, respectively. The charge on the two capacitors should equal, thus

$$C_O V_O = \frac{kk_0 S V_O}{d} = neS = \frac{\left(\frac{E_F}{\hbar v_F}\right)^2 eS}{\pi} = \frac{e^3 V_Q^2 S}{\hbar^2 v_F^2 \pi}, \tag{2}$$

where k, S, d, n, v_F are the permittivity, graphene area, SiO_2 thickness, carrier density, Fermi velocity, respectively. Here we have used the low temperature formula $n = (E_F/\hbar v_F)^2/\pi$ derived from the density of states of graphene. Solving the simultaneous Eqs. (1) and (2) gives

$$V_Q = \frac{\hbar v_F [\sqrt{\pi k k_0 (\hbar^2 v_F^2 \pi k k_0 + 4e^3 d V_g')} - \hbar v_F \pi k k_0]}{2e^3 d}. \tag{3}$$

In our device, when V_g>20 V, E_F of the gate controlled graphene is above the Dirac point and *pn* junctions are created (Fig. 4(a)). When 0 V<V_g<20 V, the graphene starts to be *p*-type. Using (3), we can estimate when V_g = 0 V (Note V_g' in Eq. (3) has to be corrected from the experimental V_g by the 20 V Dirac voltage offset), E_F is ~0.14 eV above the Dirac point (Fig. 4(d)). In Fig. 4(e), when V_g = –30 V, the Dirac point is pushed ~0.22 eV above the Dirac point. Since the gate is situated asymmetrically, the induced potential profile is also asymmetric (the slope is steeper on the right side, e.g. indicated in Fig. 4(b)). Due to the charge transfer between the metal contacts and graphene, built-in potentials are formed in the very vicinity (in the order of few 100 nm) of the electrodes (Fig. 4) [2,15]. This potential,

#262435 Received 4 Apr 2016; revised 24 May 2016; accepted 24 May 2016; published 1 Jun 2016
© 2016 OSA

however, is small under our condition (in the order of few 10 mV) [2,15], and plays a minor role in the device operation.

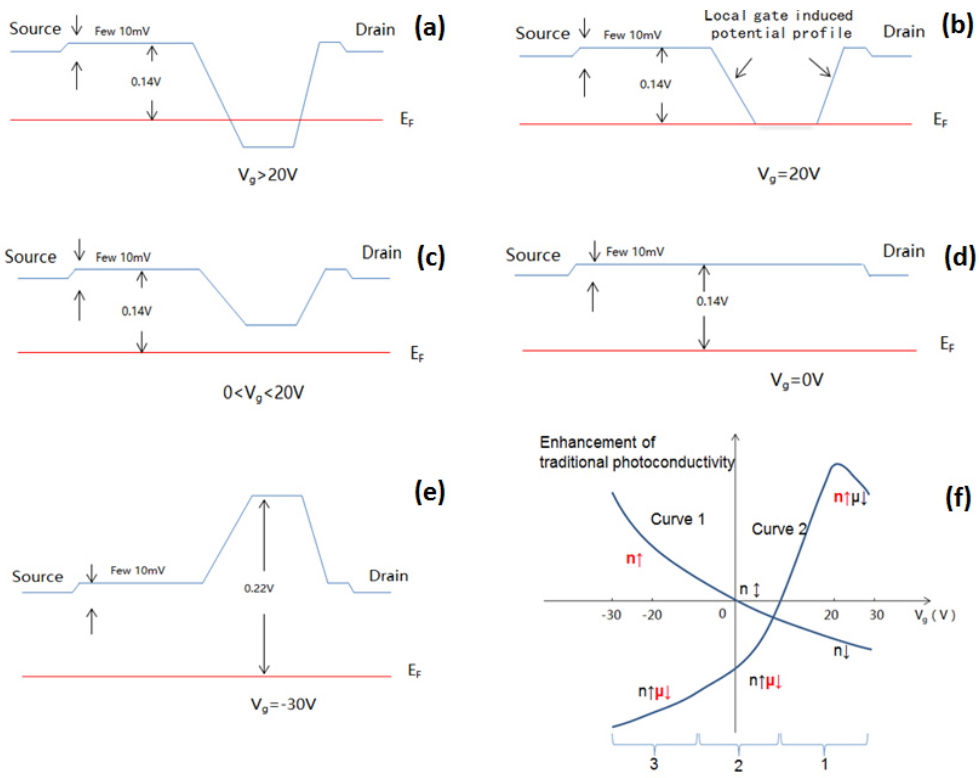

Fig. 4. (a-e) Schematic diagram of the electric potential profile along the graphene channel (the small source-drain bias is neglected for simplicity) at different regimes of V_g. There are local gate induced potentials in the device, where at the left side of the gate the field appears to be somewhat weaker than that at the right. In comparison, the built-in potentials at the graphene-metal junctions are relatively small. Also, they are symmetric at the two electrodes and the effect on the photocarrier transport will be largely canceled out. (f) Schematics of the effect on the transport from the carrier number and mobility change (curve 1) and net internal potential change (curve 2) in three gate voltage regimes. Under illumination, the carrier density n and mobility μ will be modified, as indicated by the arrows. In each V_g regime, the dominant effects are marked with red and bold font.

In Fig. 2(d), there is no detectable photo response at V_{sd} = 0 V, meaning our device does not generate any $\mathcal{E}$. Naturally, the absolute value $|I_{ph}|$ is larger when V_{sd} increases from 0.02 V to 0.04 V. When V_g is ~20 V, E_F in the graphene is tuned near the Dirac point (Fig. 4(b)). The incident light induces e-h pairs and increases the carrier density n, leading to a TP. At the same time, the device temperature increases too. As discussed in the introduction, the e-e scattering is the major relaxation process. Hence, the scattering is boosted, rendering a negative photoconductivity. The bolometric effect can be seen as a reduction of the carrier mobility μ, affecting the total photoconductivity σ_{ph} through competing with the TP (σ_{ph} = $n_{light}e\mu_{light}$-$n_{dark}e\mu_{dark}$). Nevertheless, as the number of carriers is minimal, the bolometric effect is weak. The applied V_{sd} urges the electrons to migrate rightward. As our gate induced internal potential is asymmetric, the sum of the fields yields a force pushing the electrons leftward (Fig. 4(b)). In other words, the net internal potential in the channel is not in favor of TP. It is against the effective separation of the e-h pairs, leading to reduced photocarrier lifetime ($n\downarrow$). But the influence is minor, and a clear TP is observed in Fig. 3 at V_g≈20 V (region 1 in Fig. 4(f)). In Fig. 4(f), curves 1 and 2 depict the enhancement of TP by the gate

#262435 Received 4 Apr 2016; revised 24 May 2016; accepted 24 May 2016; published 1 Jun 2016
© 2016 OSA

induced changes in carrier number/mobility and internal potential, respectively. Curve 1 describes that n increases and μ decreases when light is turned on. Curve 2 shows n decreases due to the unfavorable potential for V_g>0 V, and increases for the favorable potential at V_g<0 V. Indeed, as shown in Fig. 4(d), when V_g is ~0 V, there is no net potential. Because we are far from the Dirac point, n is large and the light induced decrease in μ becomes significant. As a result, the bolometric effect is dominant, and a negative σ_{ph} is observed in Fig. 3, corresponding to region 2 in Fig. 4(f). When V_g is very negative (region 3), the bolometric effect continues to be significant, but the net internal potential changes sign and is favorable for TP (Fig. 4(e)). It helps separate the e-h pairs and increase the photocarrier lifetime ($n\uparrow$). The bolometric effect and TP are now well-matched in strength, giving a nearly zero I_{ph} in Fig. 3. In some devices, TP can be even slightly stronger than the bolometric effect in this regime. Finally, we note that the source-drain voltage also influences the carrier concentration in the graphene channel. However, considering the small scale of V_{sd} and the fact that V_{sd} is unchanged in each measurement, this influence is ignored in the discussion.

4. Conclusion

Summarily, we have prepared graphene photodetectors by CVD and standard photolithography. The unfocused light source (790 nm laser and ordinary white LED) enlarges the photosensitive area of graphene and mimics the real-life sensing situations, giving a room temperature responsivity of 104 mA/W without special light absorbance enhancement methods. The working principles of the devices are explained by the positive photoconductivity from the classical e-h pairs and the negative photoconductivity from the bolometric effect. The buried local gate is located asymmetrically with respect to the source and drain, inducing a net internal potential in the graphene channel. The potential is not big enough to generate an electromotive force when the devices are unbiased, but can still influence the photodetective operation. The relative strength between the two kinds of photoconductivities depends on the gate voltage. Distinct from most of the previous works, our technique is scalable and compatible with existing semiconductor technology, which is a step ahead toward real applications.

Acknowledgments

The work is supported by Beijing Natural Science Foundation (4132006, 4152003), National Natural Science Foundation of China (61376049, 61575008, 61574011), Foundation of Based Technology (YXBGD20151JL01), Specialized Research Fund for the Doctoral Program of Higher Education (20121103110018), Beijing Municipal Education Commission (PXM2016_014204_500026), Stiftelsen Olle Engkvist Byggmästare, Carl Tryggers Stiftelse, Chalmers Area of Advance Nano and Energy, Stiftelsen för Internationalisering av Högre Utbildning och Forskning and Stiftelsen för Strategisk Forskning.

#262435 Received 4 Apr 2016; revised 24 May 2016; accepted 24 May 2016; published 1 Jun 2016
© 2016 OSA